Electron-lattice interaction and superconductivity in $BaPb_{1-x}Bi_xO_3$ and $Ba_xK_{1-x}BiO_3$

1990 J. Phys.: Condens. Matter 2 3553

(http://iopscience.iop.org/0953-8984/2/15/012)

J. Phys.: Condens. Matter **2** (1990) 3553–3566. Printed in the UK

Electron–lattice interaction and superconductivity in $BaPb_{1-x}Bi_xO_3$ and $Ba_xK_{1-x}BiO_3$

Masafumi Shirai, Naoshi Suzuki and Kazuko Motizuki
Department of Material Physics, Faculty of Engineering Science, Osaka University, Toyonaka 560, Japan

Received 22 August 1989

Abstract. The electron–lattice interaction of $BaPb_{1-x}Bi_xO_3$ (BPB) and $Ba_xK_{1-x}BiO_3$ (BKB) is studied microscopically by using the realistic electronic bands of $BaBiO_3$ reproduced by the tight-binding model. It is found that the electron–lattice coupling coefficients have strong wavevector and mode dependences. The electron–lattice interaction causes a remarkable renormalisation of the longitudinal oxygen stretching and/or breathing mode vibration. Superconductivity is discussed in the framework of the strong-coupling theory of the phonon mechanism. The spectral function $\alpha^2F(\omega)$ has some prominent structures in the frequency range of the oxygen stretching/breathing mode. As x increases, some of the main peaks in $\alpha^2F(\omega)$ shift to the lower-frequency side, reflecting the phonon frequency renormalisation. The transition temperature T_c and the energy gap function $\Delta(\varepsilon)$ at $T = 0$ K have been evaluated by solving the Eliashberg equations. The calculated T_c increases rapidly with increasing x, and reaches about 30 K for $x = 0.7$. The oxygen isotope shift of T_c in BKB is calculated and the characteristic exponent α defined by $T_c \propto M_O^{-\alpha}$ (M_O is oxygen atomic mass) is evaluated to be 0.35–0.45. The superconducting energy gap Δ_0 is evaluated to be 4.8 meV for $x = 0.7$. The ratio $2\Delta_0/k_BT_c$ is found to have a value close to that predicted by the Bardeen–Cooper–Schrieffer weak-coupling theory ($2\Delta_0/k_BT_c = 3.5$). However, the calculated tunnelling differential conductance dI/dV and its derivative d^2I/dV^2 show behaviours that are characteristic to the strong-coupling superconductor.

1. Introduction

The oxide superconductor $BaPb_{1-x}Bi_xO_3$ (BPB) with perovskite-type structure is a prototype of a series of high-transition-temperature (T_c) oxides. BPB exhibits a metallic behaviour in the composition range $0 \leqslant x < 0.35$ and becomes a superconductor with a relatively high T_c [1]. On the other hand, BPB shows semiconducting properties over the wide range $0.35 < x \leqslant 1$. The observed T_c shows a remarkable dependence on x and takes its maximum $T_c \simeq 12$ K around $x = 0.25$ [2], which is extraordinarily high among superconductors not containing any transition elements. Such a relatively high T_c contrasts with the experimental facts that BPB has a low carrier density $n \simeq 10^{21}$ cm^{-3} [2] or a small density of states at the Fermi level $N(E_F) \simeq 10^{-1}$ states/(eV unit cell spin) [3].

Recently $Ba_xK_{1-x}BiO_3$ (BKB) has been found to have the highest T_c ($\simeq 28$ K at $x = 0.7$) among oxide superconductors not containing Cu ions [4–6]. It should be noted that the notation of composition x differs from the usual one, i.e. $Ba_{1-x}K_xBiO_3$, for convenience in dealing with both BPB and BKB simultaneously.

0953-8984/90/153553 + 14 $03.50

An unsolved question is whether the origin or mechanism of superconductivity in high-T_c oxides is the usual phonon mechanism or not. Neither BPB nor BKB contain any transition-metal element. Hence, the magnetic mechanism may not be expected for the superconductivity in these compounds. In fact no magnetic order has been observed in BPB and BKB by the muon spin rotation experiments [7] and the magnetic susceptibility in the normal state in BPB and BKB shows a Pauli paramagnetic behaviour [8–10]. Therefore, it is quite important to make a thorough investigation of the superconductivity in BPB and BKB on the basis of the phonon mechanism.

We have already studied [11–13] microscopically the electron–lattice interaction and the lattice dynamics of BPB in the composition range $0 < x < 0.35$, and the superconducting transition temperature T_c has been estimated on the basis of the semi-empirical McMillan equation. It has been pointed out that the wavevector and mode dependences of the electron–lattice interaction would play an important role in the lattice dynamics and the superconductivity. The purpose of the present paper is, first, to extend our investigation to a wider composition range ($0 < x < 1$), which covers the superconducting composition of BKB, and, secondly, to study in detail the superconducting properties of BPB and BKB in the framework of the strong-coupling theory based on the Eliashberg equation.

In section 2 the electron–lattice interaction in BPB and BKB is studied microscopically on the basis of the realistic electronic band structure. In section 3 the lattice dynamics of these compounds is investigated by taking account of the effect of the electron–lattice interaction. In section 4 the spectral function $\alpha^2F(\omega)$ is first calculated by utilising the results obtained in sections 2 and 3, and then the transition temperature T_c, the oxygen isotope shift of T_c and the gap function $\Delta(\varepsilon)$ at $T = 0$ K are calculated by solving the Eliashberg equation. The results are compared with experiments. Finally, section 5 is devoted to a summary. Part of the present work has been reported elsewhere [14, 15].

2. Electron–lattice interaction

We have studied the electron–lattice interaction in BPB by using the realistic conduction band obtained by the tight-binding approximation [11]. The electronic band structure of BPB has been originally calculated by Mattheiss and Hamann [16] using the self-consistent scalar-relativistic linearised augmented plane-wave (LAPW) method. They have carried out the LAPW band calculation for $BaPbO_3$, $BaPb_{0.7}Bi_{0.3}O_3$ and $BaBiO_3$ in the cubic structure. According to their results the conduction bands of the above three compounds have almost the same structure. It has been shown that their conduction band consists mainly of a σ-bonding of O 2p and Pb (or Bi) 6s orbitals and that it can be well reproduced by the tight-binding (TB) model with three kinds of Slater–Koster [17] transfer integrals between nearest-neighbouring O and Pb (or Bi) atoms. Recently Matthiess and Hamann [18] calculated the band structure of the ordered alloy $Ba_{0.5}K_{0.5}BiO_3$, and it is confirmed that the conduction band of $BaBiO_3$ is little affected by substitution of K for Ba. Therefore, we use the same conduction band for both BPB and BKB, and adopt the rigid-band approximation, i.e. we assume that as x increases the TB conduction band is filled gradually without change of its dispersion. At $x = 0$ the conduction band is empty and at $x = 1$ it is half-filled. The values of the three transfer integrals used in the present work are as follows: $t(\mathrm{sp}\sigma) = 2.2$ eV, $t(\mathrm{pp}\sigma) = 2.7$ eV and $t(\mathrm{pp}\pi) = -0.9$ eV.

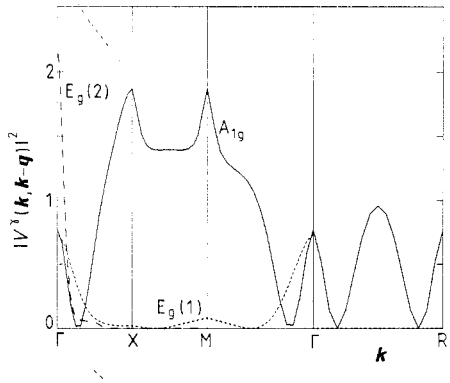

Figure 1. The electron–phonon coupling coefficient $V^\gamma(\boldsymbol{k}, \boldsymbol{k}-\boldsymbol{q})$ as a function of the wavevector $\boldsymbol{k}$ for the fixed value of $\boldsymbol{q}$ at the R point $(\pi/a, \pi/a, \pi/a)$.

In the TB approximation the electron–lattice coupling is described by the change of transfer integrals and of site energies due to atomic displacements. In this paper, however, we account only for the transfer term for simplicity because we have confirmed that the site-energy term leads to almost the same result as that of the transfer term. The coupling coefficient between two Bloch states $n\boldsymbol{k}$ and $n'\boldsymbol{k}'$ caused by displacement of the μth atom along the α direction ($\alpha = x, y, z$) is expressed as follows [19]:

$$g_\mu^\alpha(n\boldsymbol{k}, n'\boldsymbol{k}') = \sum_{\mu' a} \sum_{\nu' b} [A^\dagger(\boldsymbol{k})]_{n,\mu'\alpha} [\dot{T}_\mu^\alpha(\boldsymbol{k}, \boldsymbol{k}')]_{\mu' a, \nu' b} [A(\boldsymbol{k}')]_{\nu' b, n'}. \tag{1}$$

Here $A(\boldsymbol{k})$ represents the transformation coefficients, which diagonalise the Hamiltonian matrix of the undistorted structure, and $\dot{T}_\mu^\alpha(\boldsymbol{k}, \boldsymbol{k}')$ is written in terms of derivatives of the transfer integrals, $t'(\mathrm{sp}\sigma)$, $t'(\mathrm{pp}\sigma)$ and $t'(\mathrm{pp}\pi)$. By taking into consideration electronic band structures in a distorted phase of $BaBiO_3$ the magnitude of t' has been estimated to be about 4 eV A^{-1} [12].

The intra-band electron–phonon coupling coefficient for the conduction band can be defined by

$$V^\gamma(\boldsymbol{k}, \boldsymbol{k}-\boldsymbol{q}) = \sum_{\mu\alpha} \frac{1}{\sqrt{M_\mu}} \varepsilon_{\gamma,\mu\alpha}(\boldsymbol{q}) g_\mu^\alpha(c\boldsymbol{k}, c\boldsymbol{k}-\boldsymbol{q}). \tag{2}$$

Here γ specifies the phonon mode, $\varepsilon_{\gamma,\mu\alpha}(\boldsymbol{q})$ represents the phonon polarisation vector, M_μ is the mass of the μth atom, and c in g_μ^α denotes the conduction band. Figure 1 shows the dependences on $\boldsymbol{k}$ of $V^\gamma(\boldsymbol{k}, \boldsymbol{k}-\boldsymbol{q})$ for the fixed value of $\boldsymbol{q} = (\pi/a, \pi/a, \pi/a)$, the R point in the Brillouin zone (BZ). We have used the following values for the derivatives of the transfer integrals:

$$t'(\mathrm{sp}\sigma) = -4.05 \text{ eV A}^{-1}$$
$$t'(\mathrm{pp}\sigma) = -4.17 \text{ eV A}^{-1}$$
$$t'(\mathrm{pp}\pi) = 3.78 \text{ eV A}^{-1}.$$

As shown later, for these values the cubic structure of BPB and BKB becomes unstable for $x \geq 0.9$ against a distorted structure described as the frozen state of the so-called breathing phonon mode at the R point. Throughout this paper we use the above values for the derivatives of the transfer integrals.

As seen from figure 1 the electron–phonon coupling for the A_{1g} phonon mode (so-called breathing mode) is stronger than that for the other modes almost throughout the

Table 1. Short-range force constants (eV A^{-2}) determined from the neutron scattering measurements.

	Stretching	Bending
(Pb,Bi)–O	4.678	—
O–O	1.104	−0.055
Ba–O	0.309	—
Ba–(Pb,Bi)	1.426	—
Ba–(Ba,K)	0.129	—
(Pb,Bi)–(Pb,Bi)	0.968	—

BZ. The stretching-type deformation of $(Pb,Bi)O_6$ octahedra, which corresponds to the E_g mode, has the next strongest electron–lattice coupling. The coupling coefficients for the vibration of (Pb,Bi) atoms are almost an order of magnitude smaller than those for the A_{1g} and/or E_g modes, because the mass of (Pb,Bi) is about 13 times larger than that of O atoms. Since the conduction band states consist of the O 2p and (Pb,Bi) 6s and 6p orbitals, the vibrations of the (Ba,K) atoms cannot affect the conduction band states. The displacements of O atoms in directions tangential to nearest-neighbouring (Pb,Bi)–O bonds also have no contribution to the electron–lattice interaction as long as we take into account only the first-order coupling coefficient with respect to the atomic displacement. Hence, the coupling coefficients for the rotational and bending mode of $(Pb,Bi)O_6$ octahedra definitely become zero in the present case.

3. Lattice dynamics

We have studied the lattice dynamics, which gives important information on the role of the electron–lattice interaction in the present system. The phonon frequencies have been obtained by diagonalising the dynamic matrix $\mathbf{D}(\boldsymbol{q})$, which can be divided into two parts, $\boldsymbol{\chi}(\boldsymbol{q})$ and $\mathbf{D}^0(\boldsymbol{q})$. Here, $\boldsymbol{\chi}(\boldsymbol{q})$ represents the generalised electronic susceptibility, and the matrix elements of $\boldsymbol{\chi}(\boldsymbol{q})$ are given by

$$\chi_{\mu\nu}^{\alpha\beta}(\boldsymbol{q}) = -2\sum_{\boldsymbol{k}} g_{\mu}^{\alpha}(c\boldsymbol{k}, c\boldsymbol{k}-\boldsymbol{q}) g_{\nu}^{\beta}(c\boldsymbol{k}, c\boldsymbol{k}-\boldsymbol{q})^* \frac{f(E_{k-q}^0)-f(E_k^0)}{E_k^0 - E_{k-q}^0} \tag{3}$$

where $g_{\mu}^{\alpha}(c\boldsymbol{k}, c\boldsymbol{k}-\boldsymbol{q})$ is the electron–lattice coupling coefficient for the conduction band, E_k^0 denotes the conduction band energy in the undistorted structure and $f(E_k^0)$ is the Fermi distribution function. The Fourier transform of $\chi_{\mu\nu}^{\alpha\beta}(\boldsymbol{q})$ corresponds to the effective long-range interatomic force caused by the electron–lattice interaction. On the other hand, $\mathbf{D}^0(\boldsymbol{q})$ denotes contributions other than $\boldsymbol{\chi}(\boldsymbol{q})$. Usually $\mathbf{D}^0(\boldsymbol{q})$ is expressed as the Fourier transform of interatomic short-range forces.

First, we have calculated phonon frequencies $\omega_{q\gamma}^0$ with neglect of $\boldsymbol{\chi}(\boldsymbol{q})$. For short-range forces we have considered the stretching force for six kinds of nearest-neighbouring atomic pairs and the tangential force for one kind of nearest-neighbouring atomic pair. The seven force constants in total have been determined so as to reproduce seven phonon frequencies observed in $BaPb_{0.75}Bi_{0.25}O_3$ by inelastic neutron scattering measurements [20] (full circles in figure 2(*a*)). The short-range force constants thus determined are listed in table 1. Since Pb and Bi atoms are next door to each other in

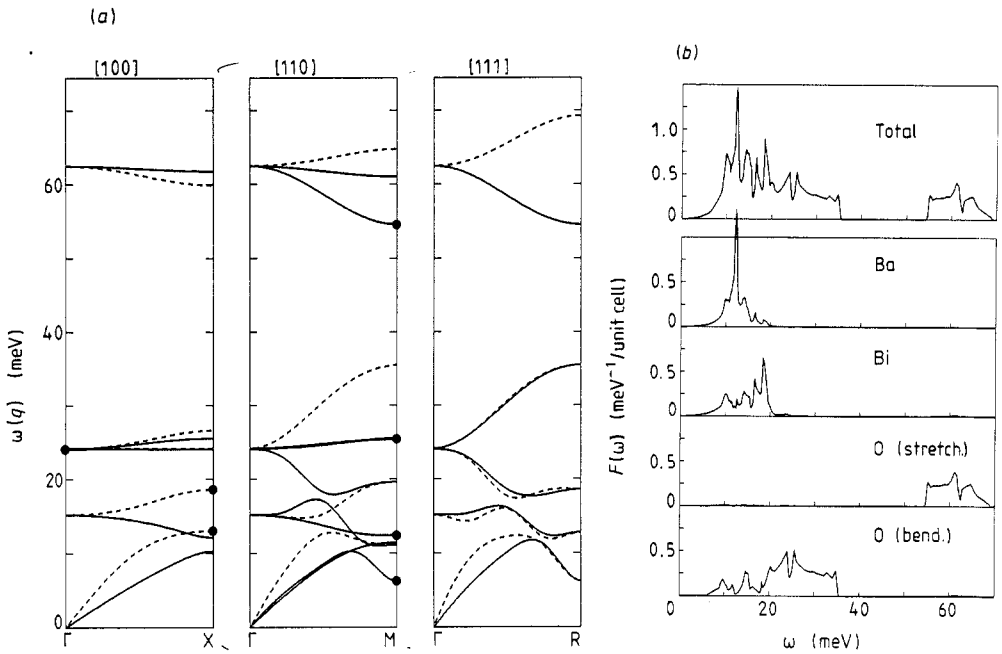

Figure 2. (*a*) The phonon dispersion curves calculated with neglect of $\chi(q)$. The full curves represent the transverse mode and the broken curves the longitudinal mode. The full circles indicate the experimental data utilised in determining the short-range force constants. (*b*) The phonon density of states neglecting $\chi(q)$. Four kinds of decomposed density of states are also shown.

the periodic table, we have regarded Pb and Bi as the same atom and neglected the effect of the randomness.

The phonon dispersion curves calculated along the (100), (110) and (111) directions are shown in figure 2(*a*) and the phonon density of states is shown in figure 2(*b*). The frequencies of oxygen stretching vibration towards the nearest-neighbouring Pb (or Bi) atoms lie around 60 meV and those of oxygen bending modes extend in the range from 10 to 35 meV. The frequencies of phonon modes arising mainly from Ba atoms lie around 15 meV. Vibrations of Pb (or Bi) atoms are mainly included in acoustic branches up to 20 meV.

In BKB the atomic masses of Ba and K are quite different and hence we have to take into account the effect of the randomness. Further, for nearest-neighbouring K–O, K–Bi and K–K pairs we should use force constants different from those for nearest-neighbouring Ba–O, Ba–(Pb,Bi) and Ba–Ba pairs. As noted in section 2, however, vibrations of Ba or K atoms are hardly coupled with the conduction band states. Further, the vibrations of O atoms, which are shown later to play an important role in the superconductivity, are little affected by the short-range force constants associated with Ba or K atoms. Therefore, in the following we neglect the difference between Ba and K atoms in BKB and use the short-range force constants associated with Ba atoms in table 1 even for those associated with K atoms.

Next we have calculated the phonon dispersion curves by including the generalised electronic susceptibility $\chi(q)$ into the dynamic matrix $\mathbf{D}(q)$. The dispersion curves and

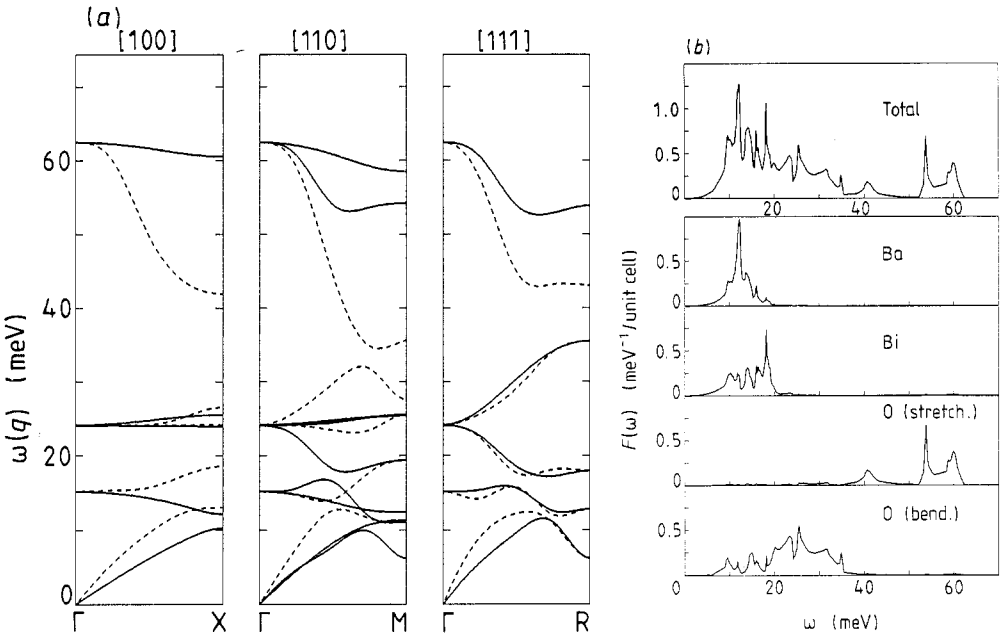

Figure 3. (*a*) The phonon dispersion curves and (*b*) the phonon density of states calculated including $\chi(q)$ for $x = 0.7$.

the density of states $F(\omega)$ calculated for $x = 0.7$ are shown in figures 3(*a*) and (*b*), respectively. By comparing figures 2(*a*) and 3(*a*) it is seen that the electron–lattice interaction causes a remarkable energy renormalisation for the longitudinal (L) mode of oxygen stretching and/or breathing vibrations whose bare frequencies lie near 60 meV. The phonon frequency renormalisation shows remarkable wavevector dependences. For $x = 0.7$, remarkable renormalisation is found near the BZ boundary especially around the M and R points. It originates from the nesting effect of the Fermi surface as well as the remarkable wavevector dependences of the electron–phonon coupling shown in figure 1. The overall features of the phonon density of states in figure 3(*b*) are in agreement with the results of molecular dynamics simulation and of neutron scattering measurements [21], except for the high-frequency range between 60 and 80 meV.

The magnitude of the renormalisation of the longitudinal (L) oxygen (O) stretching/breathing mode increases on increasing the value of x. For $x \geq 0.9$ the O breathing phonon at the R point vanishes and hence the lattice becomes unstable against formation of the distorted structure described by that phonon. Experimentally the structure of $BaBiO_3$ at room temperature has been confirmed to be described by a frozen state of the O breathing phonon just at the R point [22].

Mysteriously the energies of the L O stretching/breathing mode have not been detected in the neutron scattering experiments in $BaPb_{0.75}Bi_{0.25}O_3$ [20]. Instead, rather broad peaks were observed near the BZ boundary in the energy region of 40–45 meV. A reason why the phonon mode cannot be detected is considered as broadening of the phonon linewidth because of the strong electron–lattice interaction. Thus, phonon linewidth caused by the electron–lattice interaction is calculated microscopically. The

phonon linewidth is related to the imaginary part of the polarisation function. If we evaluate the polarisation function in the Migdal approximation [23], then the phonon linewidth is expressed as [24]

$$\Gamma_{q\gamma} = \pi \sum_{k} |V^{\gamma}(\boldsymbol{k}, \boldsymbol{k}-\boldsymbol{q})|^2 \delta(E_k^0 - E_F)\delta(E_{k-q}^0 - E_F). \tag{4}$$

We have found that the L O stretching/breathing mode phonons broaden significantly because of the strong electron–lattice interaction. The L O stretching/breathing mode phonons have linewidth several orders of magnitude larger than that of the other modes. Especially near the M point where the phonon frequencies are renormalised most significantly, the full width becomes at most about 14 meV for $x = 0.7$.

4. Superconductivity

4.1. Spectral function $\alpha^2F(\omega)$

To discuss the superconductivity of BKB and BPB in the framework of the strong-coupling theory based on the phonon mechanism, we first calculate the spectral function $\alpha^2F(\omega)$ defined by

$$\alpha^2F(\omega) = \frac{1}{N(E_F)} \sum_{k} \sum_{k'} \sum_{\gamma} \frac{|V^{\gamma}(\boldsymbol{k}, \boldsymbol{k}')|^2}{2N\omega_{k'-k}^{\gamma}} \delta(E_k^0 - E_F)\delta(E_{k'}^0 - E_F)\delta(\omega - \omega_{k'-k}^{\gamma}) \tag{5}$$

where $V^{\gamma}(\boldsymbol{k}, \boldsymbol{k}')$ is the electron–phonon coupling coefficient defined by equation (2), and ω_q^{γ} denotes the renormalised phonon frequency. The calculated $\alpha^2F(\omega)$ is shown by full curves in figure 4, together with the phonon density of states $F(\omega)$ (broken curves). It is found that $\alpha^2F(\omega)$ has a frequency dependence entirely different from that of $F(\omega)$. It should be noted that $\alpha^2F(\omega)$ has some prominent structures in the frequency range where O stretching/breathing mode branches lie. Thus, the O stretching/breathing mode is expected to contribute dominantly to the superconductivity. As x increases, some main peaks in $\alpha^2F(\omega)$ shift to the lower-energy side, reflecting the phonon frequency renormalisation, and the magnitude of $\alpha^2F(\omega)$ increases remarkably in the whole energy range up to 60 meV. This considerable change in $\alpha^2F(\omega)$ is expected to bring a remarkable dependence on x of T_c.

The dimensionless coupling constant λ is evaluated by integrating $\alpha^2F(\omega)$ as

$$\lambda = 2\int_0^{\infty} \frac{\alpha^2F(\omega)}{\omega} \mathrm{d}\omega. \tag{6}$$

The results are shown as a function of x in figure 5. It is found that λ increases rapidly with increasing x, especially for $x > 0.5$. This behaviour is due to the renormalisation of the O stretching/breathing mode phonons. Finally, λ exceeds 1.0 for $x > 0.7$, which indicates that BKB belongs to the strong-coupling superconductors. Recent heat capacity measurements for $Ba_{0.6}K_{0.4}BiO_3$ [25] revealed that the electronic specific heat coefficient was $\gamma = 1.5$ mJ mol^{-1} K^{-2}. Then, from the relation $\gamma = \frac{1}{3}\pi^2N(E_F)k_B^2(1 + \lambda)$ with use of the calculated value of $N(E_F) = 0.23$ states/(eV unit cell spin), λ is estimated to be 0.35, which is smaller than the theoretical value $\lambda = 0.8$ obtained for $x = 0.6$. The reason for this discrepancy is not clear at present.

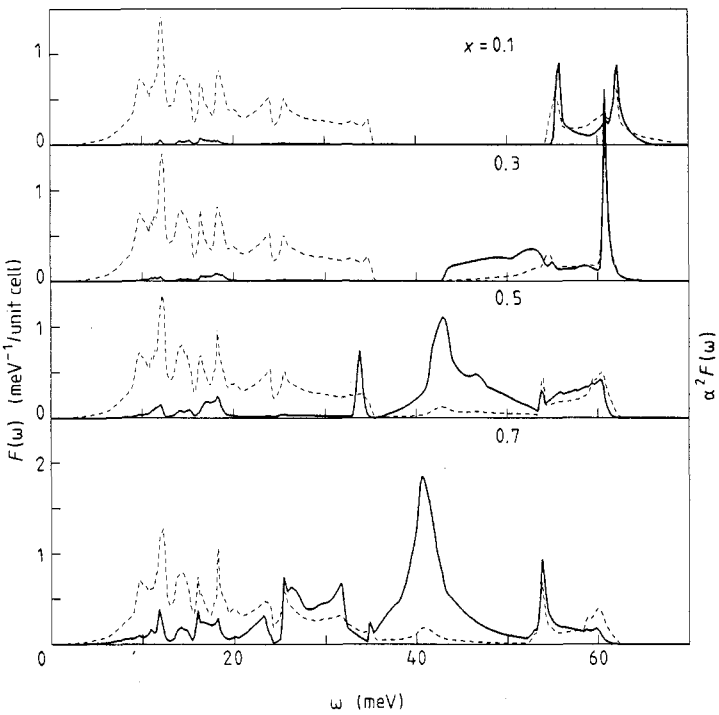

Figure 4. The spectral function $\alpha^2F(\omega)$ (full curves) and the phonon density of states $F(\omega)$ (broken curves) calculated for $x = 0.1, 0.3, 0.5$ and 0.7. $\alpha^2F(\omega)$ is a dimensionless quantity.

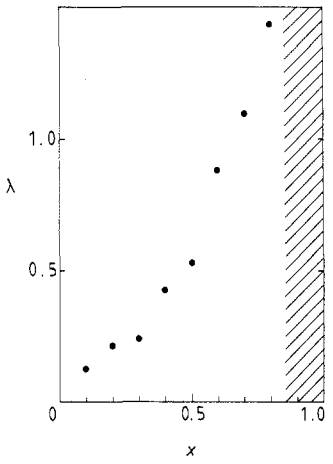

Figure 5. The dimensionless electron–phonon coupling constant λ evaluated as a function of x. The hatched area represents the region where the lattice becomes unstable against formation of a CDW corresponding to the frozen state of the O breathing mode at the R point.

4.2. Transition temperature and isotope effect

The superconducting transition temperature T_c is determined by solving the Eliashberg equation at finite temperatures [26]. It is much more convenient for numerical calculations to solve the 'imaginary-axis' version of the Eliashberg equation, which is defined on Matsubara imaginary frequencies $i\varepsilon_n = (2n + 1)\pi i k_B T$ (n is an integer). At

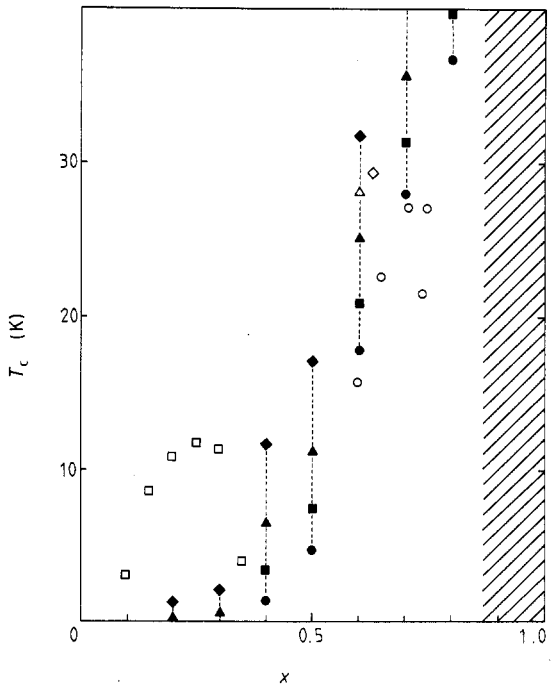

Figure 6. The superconducting transition temperature T_c as a function of x for $\mu^* = 0$ (◆), 0.05 (▲), 0.10 (■) and 0.15 (●), respectively. The experimental data for BPB, (□) [2], and for BKB, (○) [6], (△) [9], (◇) [33], are also shown. The hatched area denotes the region where the lattice becomes unstable against formation of a CDW corresponding to the frozen state of the O breathing mode at the R point.

any temperature $T < T_c$ the Eliashberg equation is a set of non-linear coupled equations. When the temperature approaches T_c, however, the coupled equations can be decoupled and expanded with respect to the gap function $\Delta(i\varepsilon_n)$ as follows [27]:

$$\Delta(i\varepsilon_n) = \pi k_B T \sum_m \frac{\lambda(\varepsilon_n - \varepsilon_m) - \mu^*}{|\tilde{\varepsilon}_m|} \Delta(i\varepsilon_m) \tag{7}$$

where μ^* is the effective screened Coulomb repulsion constant [28],

$$\tilde{\varepsilon}_m = \varepsilon_m + \pi k_B T \sum_l \mathrm{sgn}(\varepsilon_l)\lambda(\varepsilon_m - \varepsilon_l) \tag{8}$$

and

$$\lambda(\varepsilon_n) = \int_0^\infty d\Omega\, \alpha^2 F(\Omega) \frac{2\Omega}{\Omega^2 + \varepsilon_n^2}. \tag{9}$$

Therefore, T_c can be determined so that the linearised gap equation (7) has any non-trivial solution for $\Delta(i\varepsilon_n)$ at $T = T_c$:

$$\det \left| \pi k_B T_c \frac{\lambda(\varepsilon_n - \varepsilon_m) - \mu^*}{|\tilde{\varepsilon}_m|} - \delta_{mn} \right| = 0. \tag{10}$$

In calculating T_c the dimension of the matrix in the determinant of equation (10) has been cut off at 200. The obtained dependence of T_c on x is shown in figure 6. For each x, we have calculated T_c with four different values of $\mu^* = 0, 0.05, 0.10$ and 0.15. In most superconductors μ^* has been taken empirically to be between 0.10 and 0.15. The calculated T_c increases rapidly with increasing x as long as lattice instability does not

Table 2. Calculated oxygen isotope effect on T_c. Values of the characteristic exponent α, defined by $T_c \propto M_O^{-\alpha}$ (M_O is mass of an oxygen atom), are given.

	x		
μ^*	0.5	0.6	0.7
0	0.42	0.43	0.45
0.05	0.40	0.41	0.44
0.10	0.39	0.40	0.43
0.15	0.36	0.38	0.42

occur, and reaches 31.3 K for $x = 0.7$ ($\lambda = 1.09, \mu^* = 0.1$). In the present case the lattice becomes unstable against charge-density-wave (CDW) formation for $x \geqslant 0.9$. Thus, the superconducting state of BKB is bordered by the CDW state. Our results for T_c agree well with the observed T_c in BKB, but disagree with those in BPB. One of the reasons for this discrepancy in BPB may be that the rigid-band model is insufficient to describe BPB, because in BPB the Pb atom, which is one of the constitutive elements of the conduction band, is substituted randomly by the Bi atom.

It should be noted here that one must be careful in using the McMillan [29] or Allen–Dynes [30] equation for T_c. The latter is given by

$$T_c = \frac{\langle\omega\rangle}{1.2}\exp\left(\frac{-1.04(1+\lambda)}{\lambda - \mu^*(1+0.62\lambda)}\right) \tag{11}$$

where $\langle\omega\rangle$ denotes the average phonon frequency defined by

$$\ln\langle\omega\rangle \equiv \int_0^\infty d\omega\,\frac{\alpha^2F(\omega)}{\omega}\ln\omega \Big/ \int_0^\infty d\omega\,\frac{\alpha^2F(\omega)}{\omega}. \tag{12}$$

By using the calculated $\alpha^2F(\omega)$, $\langle\omega\rangle$ is evaluated to be 28 meV for $x = 0.7$. If we use this value of $\langle\omega\rangle$ and the value of $\lambda = 1.09$ for $x = 0.7$, T_c is calculated to be 26 K from equation (11). Therefore the Allen–Dynes equation gives relatively accurate T_c as long as we use the value of $\langle\omega\rangle$ evaluated appropriately. However, if we use $F(\omega)$ of the Debye model with the observed Debye temperature $\Theta_D \simeq 280$ K [31] instead of $\alpha^2F(\omega)$ in equation (12), then $\langle\omega\rangle \simeq 0.605k_B\Theta_D \simeq 14$ meV and T_c is calculated to be 13 K, which is much smaller than that obtained directly from the Eliashberg equation. Thus, one should carefully evaluate the value of $\langle\omega\rangle$ when using the Allen–Dynes equation for the evaluation of T_c.

Next, the isotope shift of T_c has been estimated by calculating T_c when ^{16}O is replaced with ^{17}O and ^{18}O. A characteristic exponent α, defined as $T_c \propto M_O^{-\alpha}$ (M_O is oxygen atomic mass), is evaluated from the slope of the $\ln T_c$ versus $\ln M_O$ plots. The evaluated exponents α for $x = 0.5$, 0.6 and 0.7 are listed in table 2. It is found that α takes rather smaller values than the co-called Bardeen–Cooper–Schrieffer (BCS) value ($\alpha = 0.5$) [32]. Experimentally the value of α is estimated to be 0.21 by Batlogg *et al* [9], 0.35 by Kondoh *et al* [10] and 0.41 by Hinks *et al* [33]. The principal reason why α differs from the BCS value is that the vibrations of atoms other than oxygens, such as Bi atoms, contribute appreciably to the superconductivity, particularly in the case where a substantial phonon frequency renormalisation is caused by the electron–lattice interaction. Barbee *et al* [34] have carried out calculations of α in $La_{1.85}Sr_{0.15}CuO_4$ by using a simplified model spectral

function. They also have pointed out the possibility that the value of α can be much smaller than the BCS value for specific isotopic substitutions in compound superconductors.

4.3. Energy gap at T = 0 K and tunnelling spectra

Tunnelling measurement is a powerful method that can observe directly the superconducting energy gap. Schrieffer *et al* [35] have shown that the differential conductances dI/dV through the junction between the superconductor and the normal metal is proportional to the electronic density of states $N_s(\varepsilon)$ in the superconducting state as

$$\left.\frac{dI}{dV}\right|_{eV=\varepsilon} \propto \frac{N_s(\varepsilon)}{N(E_F)} = \mathrm{Re}\left(\frac{|\varepsilon|}{[\varepsilon^2 - \Delta(\varepsilon)^2]^{1/2}}\right) \tag{13}$$

where $N(E_F)$ denotes the electronic density of states at the Fermi level E_F in the normal state, and $\Delta(\varepsilon)$ represents the energy-dependent gap function at $T = 0$ K. Here, $\Delta(\varepsilon)$ is determined by solving the Eliashberg equation for $T = 0$ K and it is given [36] by

$$\xi(\varepsilon) = [1 - Z(\varepsilon)]\varepsilon = \int_{\Delta_0}^{\infty} d\varepsilon' \, \mathrm{Re}\left(\frac{\varepsilon'}{[\varepsilon'^2 - \Delta(\varepsilon')^2]^{1/2}}\right)$$
$$\times \int_0^{\infty} d\omega \, \alpha^2 F(\omega) \left(\frac{1}{\varepsilon' + \varepsilon + \omega - i\delta} - \frac{1}{\varepsilon' - \varepsilon + \omega - i\delta}\right) \tag{14}$$

and

$$\Delta(\varepsilon) = \frac{1}{Z(\varepsilon)} \int_{\Delta_0}^{\infty} d\varepsilon' \, \mathrm{Re}\left(\frac{\varepsilon'}{[\varepsilon'^2 - \Delta(\varepsilon')^2]^{1/2}}\right)$$
$$\times \int_0^{\infty} d\omega \, \alpha^2 F(\omega) \left(\frac{1}{\varepsilon' + \varepsilon + \omega - i\delta} + \frac{1}{\varepsilon' - \varepsilon + \omega - i\delta}\right)$$
$$- \frac{\mu^*}{Z(\varepsilon)} \int_{\Delta_0}^{\varepsilon_c} d\varepsilon' \, \mathrm{Re}\left(\frac{\varepsilon'}{[\varepsilon'^2 - \Delta(\varepsilon')^2]^{1/2}}\right) \qquad (\delta \to +0). \tag{15}$$

Here $\xi(\varepsilon)$ is the electronic self-energy of the normal state, $Z(\varepsilon) \equiv 1 - \xi(\varepsilon)/\varepsilon$ is called the mass enhancement function, and Δ_0 is defined by $\Delta_0 = \Delta(\Delta_0)$, which denotes the superconducting energy gap.

Once the spectral function $\alpha^2F(\omega)$ and μ^* are given, $\xi(\varepsilon)$ and $\Delta(\varepsilon)$ are calculated by utilising equations (14) and (15) in a self-consistent manner. In actual calculations the cut-off energy ε_c has been taken to be 200 meV and $\Delta(\varepsilon)$ has converged sufficiently in several iterations. The obtained $Z(\varepsilon)$ and $\Delta(\varepsilon)$ for $x = 0.7$ and $\mu^* = 0.1$ are shown in figures 7(*a*) and (*b*), respectively. It is found that the real part of the renormalisation function $Z(\varepsilon)$ has some small peaks up to 60 meV, which correspond to the peaks in $\alpha^2F(\omega)$. On the other hand, $\Delta(\varepsilon)$ has sharp and prominent structures reflecting the peaks in $\alpha^2F(\omega)$, and the structures are extended to the higher-energy range above 60 meV. The superconducting energy gap Δ_0 is found to be 4.8 meV. This result is in good agreement with the recent optical measurements [37], which show $\Delta_0 = 4.4$ meV. Since T_c has been evaluated to be 31.3 K for $x = 0.7$ and $\mu^* = 0.1$, the ratio $2\Delta_0/k_BT_c$ is found to be about 3.6, which is accidentally close to that predicted by the BCS theory ($2\Delta_0/k_BT_c = 3.5$).

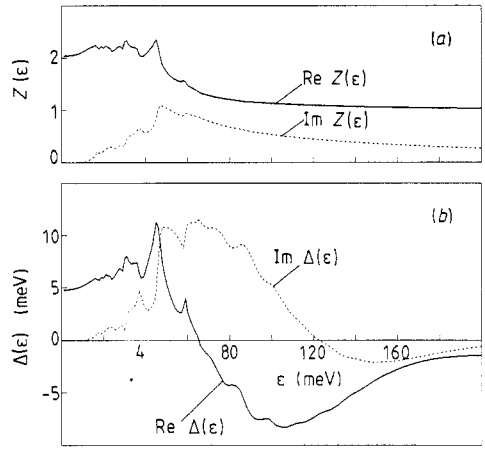

Figure 7. (*a*) The renormalisation function $Z(\varepsilon)$ and (*b*) the gap function $\Delta(\varepsilon)$ determined by solving the Eliashberg equation at $T = 0$ K for $x = 0.7$ and $\mu^* = 0.1$.

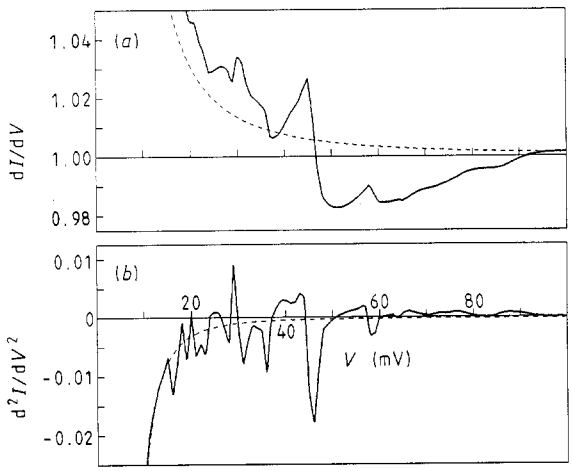

Figure 8. (*a*) The differential conductance dI/dV and (*b*) its derivative d^2I/dV^2 calculated for $x = 0.7$ and $\mu^* = 0.1$. The broken curves represent the results obtained by using the BCS weak-coupling theory.

Such prominent structures in $\Delta(\varepsilon)$ as shown in figure 7(*b*) can be observed by the tunnelling experiments. The differential conductance dI/dV calculated from equation (13) is shown by the full curve in figure 8(*a*) together with the BCS result (broken curve), which is given by

$$\frac{N_s(\varepsilon)}{N(E_F)} \simeq \mathrm{Re}\left(\frac{|\varepsilon|}{(\varepsilon^2 - \Delta_0^2)^{1/2}}\right). \tag{16}$$

Apparent deviations from the BCS result are clearly seen in figure 8(*a*). Figure 8(*b*) shows the derivative of the differential conductance, d^2I/dV^2. In general d^2I/dV^2 gives direct information about $\alpha^2F(\omega)$, i.e. negative peaks (dips) in d^2I/dV^2 correspond to peaks in $\alpha^2F(\omega)$. Recently, tunnelling spectroscopy measurements with high resolution have been performed on $Ba_{0.625}K_{0.375}BiO_3$ ($T_c = 29$ K) [38]. The observed curves of dI/dV and d^2I/dV^2 have lineshapes similar to those shown in figures 8(*a*) and (*b*), respectively.

5. Summary

First, the electron–lattice interaction of BPB and BKB has been calculated microscopically by using the realistic electronic band structure reproduced by the tight-binding approximation. We have confirmed that the vibrations of oxygen atoms along the direction toward the nearest-neighbouring Pb or Bi atoms have strong coupling with the conduction band states. Such a mode dependence of the electron–lattice coupling arises from the nature of the conduction band states, i.e. the conduction band states consist mainly of the 6s and 6p orbitals of Pb or Bi atoms and the 2p orbitals of O atoms.

Next, we have investigated the lattice dynamics of BPB and BKB by taking account of the effect of the electron–lattice interaction. It has been found that the electron–lattice interaction causes remarkable renormalisation of the longitudinal (L) O stretching and/or breathing mode phonons especially near the Brillouin zone boundary. The phonon frequencies of these modes become lower and lower with increasing number of conduction electrons or composition x. Finally lattice instability occurs accompanied by vanishing of these phonon frequencies. We have also found a broadening of linewidth for the renormalised phonons, which might be related to the absence of those phonon modes in the neutron scattering measurement.

Further, the superconductivity of BPB and BKB has been discussed in the framework of the strong-coupling theory of the phonon mechanism. We have obtained the following results.

(i) The spectral function $\alpha^2F(\omega)$ takes large values in the frequency range where the L O stretching/breathing mode phonons lie, which implies the importance of these phonons for the superconductivity.

(ii) The transition temperature T_c has been calculated by solving the Eliashberg equation. It is found that T_c increases rapidly with increasing x, and reaches 30 K around $x = 0.7$. The obtained dependence of T_c on x agrees well with that observed in BKB.

(iii) The isotope shift of T_c has been investigated by calculating T_c when ^{16}O is replaced with ^{17}O and ^{18}O. The characteristic exponent α defined by $T_c \propto M_O^{-\alpha}$ has a rather small value between 0.35 and 0.45 compared with that predicted by the BCS theory ($\alpha = 0.5$). The results agree well with the experimental data obtained by Kondoh *et al* [10] ($\alpha = 0.35$) and/or by Hinks *et al* [33] ($\alpha = 0.41$).

(iv) The gap function $\Delta(\varepsilon)$ has been calculated for $T = 0$ K. The superconducting energy gap Δ_0 is estimated to be 4.8 meV for $x = 0.7$, which is in good agreement with the result obtained by optical measurements [37]. The ratio $2\Delta_0/k_BT_c$ is found to have a value close to that predicted by the BCS weak-coupling theory ($2\Delta_0/k_BT_c = 3.5$). However, the tunnelling differential conductance dI/dV turns out to show the behaviour that is characteristic to the strong-coupling superconductor.

Our results suggest that the superconducting properties in BKB, such as the magnitude of T_c, the isotope shift of T_c, the energy gap Δ_0 and the tunnelling spectrum, can be understood within the strong-coupling theory of the phonon mechanism. It is particularly emphasised that the significant renormalisation of the L O stretching/breathing mode phonons plays an important role for the high T_c in BKB. On the other hand, it is a further problem whether the superconductivity in BPB can be explained within the phonon mechanism. It seems that effects of random substitution of Bi for Pb have to be taken into account.

Acknowledgment

This work is supported by a Grant-in-Aid of Scientific Research on Priority Areas (No. 63631007) from the Ministry of Education, Science and Culture, Japan.

References

[1] Sleight A W, Gilson J L and Bierstedt P E 1975 *Solid State Commun.* **17** 27
[2] Thanh T D, Koma A and Tanaka S 1980 *Appl. Phys.* **22** 205
[3] Itoh T, Kitazawa K and Tanaka S 1984 *J. Phys. Soc. Japan* **53** 2668
[4] Mattheiss L F, Gyorgy E M and Johnson D W Jr 1988 *Phys. Rev.* B **37** 3745
[5] Cava R J, Batlogg B, Krajewski J J, Farrow R, Rupp L W Jr, White A E, Short K, Peck W F and Kometani T 1988 *Nature* **332** 814
[6] Hinks D G, Dabrowski B, Jorgensen J D, Mitchell A W, Richards D R, Pei S and Shi D 1988 *Nature* **333** 836
[7] Uemura Y J, Sternlieb B J, Cox D E, Brewer J H, Kadono R, Kempton J R, Kiefl R F, Kreitzman S R, Luke G M, Mulhern P, Riseman T, Williams D L, Kossler W J, Yu X H, Stronach C E, Subramanian M A, Gopalakrishnan J and Sleight A W 1988 *Nature* **335** 151
[8] Uchida S, Hasegawa H, Kitazawa K and Tanaka S 1988 *Physica* C **156** 157
[9] Batlogg B, Cava R J, Rupp L W Jr, Mujsce A M, Krajewski J J, Remeika J P, Peck W F Jr, Cooper A S and Espinoza G P 1988 *Phys. Rev. Lett.* **61** 1670
[10] Kondoh S, Sera M, Ando Y and Sato M 1989 *Physica* C **157** 469
[11] Shirai M, Suzuki N and Motizuki K 1986 *Solid State Commun.* **60** 346
[12] Shirai M, Suzuki N and Motizuki K 1988 *Japan. J. Appl. Phys. Ser.* **1** (*Supercond. Mater.*) 225
[13] Shirai M, Suzuki N and Motizuki K 1989 *Ferroelectrics* **96** 99
[14] Shirai M, Suzuki N and Motizuki K 1989 *J. Phys.: Condens. Matter* **1** 2939
[15] Shirai M, Suzuki N and Motizuki K 1990 *Phonons 89* ed S Hurklinger, W Ludwig and G Weiss (Singapore: World Scientific) p 268
[16] Mattheiss L F and Hamann D R 1983 *Phys. Rev.* B **28** 4227
[17] Slater J C and Koster G F 1954 *Phys. Rev.* **94** 1498
[18] Mattheiss L F and Hamann D R 1988 *Phys. Rev. Lett.* **60** 2681
[19] Morizuki K and Suzuki N 1986 *Structural Phase Transitions in Layered Transition-Metal Compounds* ed K Motizuki (Dordecht: Reidel) p 1
[20] Reichardt W and Weber W 1987 *Japan. J. Appl. Phys.* **26** Suppl. 3, 1121
[21] Loong C K, Vashishta P, Kalia R K, Degani M H, Price D L, Jorgensen J D, Hinks D G, Dabrowski B, Mitchell A W, Richards D R and Zheng Y 1989 *Phys. Rev. Lett.* **62** 2628
[22] Cox D E and Sleight A W 1976 *Solid State Commun.* **19** 969
[23] Migdal A B 1958 *Sov. Phys.–JETP* 7 996
[24] Allen P B 1972 *Phys. Rev.* B **6** 2577
[25] Graebner J E, Schneemeyer L F and Thomas J K 1989 *Phys. Rev.* B **39** 9682
[26] Eliashberg G M 1961 *Sov. Phys.–JETP* **12** 1000
[27] Bergmann G and Rainer D 1973 *Z. Phys.* **263** 59
[28] Morel P and Anderson P W 1962 *Phys. Rev.* **125** 1263
[29] McMillan W L 1968 *Phys. Rev.* **167** 331
[30] Allen P B and Dynes R C 1975 *Phys. Rev.* B **12** 905
[31] Hundley M F, Thompson J D and Kwei G H 1989 *Solid State Commun.* **70** 1155
[32] Bardeen J, Cooper L N and Schrieffer J R 1957 *Phys. Rev.* **108** 1175
[33] Hinks D G, Richards D R, Dabrowski B, Marx D T and Mitchell A W 1988 *Nature* **335** 419
[34] Barbee T W III, Cohen M L, Bourne L C and Zettl A 1988 *J. Phys. C: Solid State Phys.* **22** 5977
[35] Schrieffer J R, Scalapino D J and Wilkins J W 1963 *Phys. Rev. Lett.* **10** 336
[36] McMillan W L and Rowell J M 1965 *Phys. Rev. Lett.* **14** 108
[37] Schlesinger Z, Collins R T, Calise J A, Hinks D G, Mitchell A W, Zheng Y, Dabrowski B, Bickers N E and Scalapino D J 1989 *Phys. Rev.* B **40** 6862
[38] Zasadzinski J F, Tralshawala N, Hinks D G, Dabrowski B, Mitchell A W and Richards D R 1989 *Physica* C **158** 519